

# Computational Tracking of Tumor - Can the CAT catch the Mouse

S. S. Iyengar<sup>1</sup>, Xin Li<sup>1</sup>, Amit Sawant<sup>2</sup>, Huanhuan Xu<sup>1</sup>, Puneeth Iyengar<sup>2</sup>

<sup>1</sup> Louisiana State University

<sup>2</sup> University of Texas Southwestern Medical Center

## 1. Introduction

More than half of all solid tumors receive external beam ionizing radiation as part of multimodality treatment. The goal of radiation treatment is to treat disease while avoiding normal tissue toxicity. In many sites, dose escalation has been shown to offer local tumor control benefits. This has often been reported in the literature addressing irradiation of lung tumors. Lung cancer is the second most common cancer in both men and women in the United States, and people with lung cancer tend not to live long after diagnosis. Its radiation treatment therefore attracts great attention. Due to the spatial relationship of lung tumors with important normal tissue structures – spinal cord, esophagus, heart, brachial plexus, normal lung parenchyma, bronchial tree, and trachea among others – dose escalation is often not feasible to a great extent. Furthermore, radiation treatment planning for lung cancers is often complicated by complex motion of tumors during all phases of the respiratory cycle. This tumor motion and object deformity is also heavily influenced by the motion of intrathoracic normal tissue structures. Hence, for a number of reasons, treatment planning for intrathoracic radiation requires better tools to optimize precision and accuracy of delivery.

## 2. Background and Challenges

With mounting scientific evidence on both the benefits of dose escalation and the perils of normal tissue toxicity, and tremendous progress in the attainable precision of radiotherapy (RT) planning and delivery, achieving a high degree of geometric accuracy of the temporarily deforming organ has become ever more important in RT treatments. This requirement is especially critical in lung cancer RT where respiratory motion causes thoracic anatomy to change continuously in all four dimensions (4D = 3D space + time). The ideal RT guidance requires complete spatiotemporal knowledge of the moving and deforming irradiated volume (IV). However, one of the weakest aspects of current RT-guidance remains pre-treatment imaging, which is typically performed using 4D computed tomography (4DCT). A 4DCT scan is generated by acquiring CT projections over several respiratory cycles. The projections are resorted into several bins using an external motion monitor, based on the respiratory phase (phase sorting) [1], or the displacement (amplitude sorting) [2] and a time series of 3D volumes is generated. This series describes the motion of the volume over a single “representative” cycle. Typically, a maximum- or average-intensity projection (MIP or AIP), obtained from the superposition (MIP) or average (AIP) from all phases is used to define a motion-inclusive internal target volume (ITV) [3]. This ITV is used to create a treatment plan, which serves as the ground truth for all subsequent RT stages.

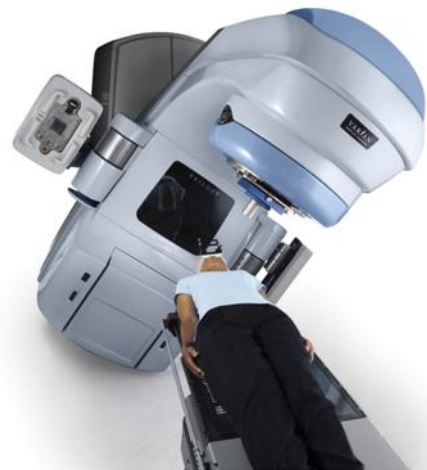


**Figure 1.** A patient being treated with external beam radiotherapy using a Varian linear accelerator.

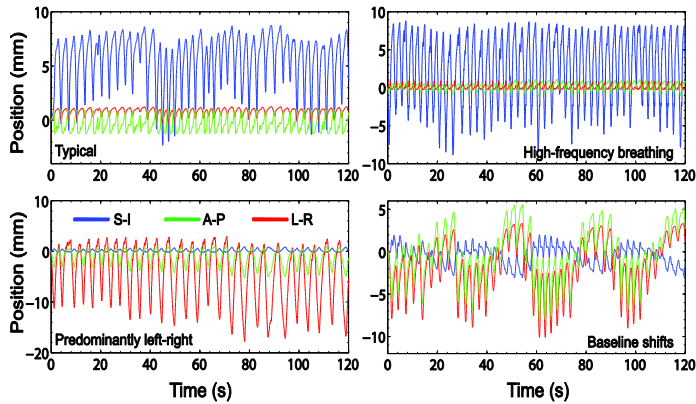


**Figure 2.** Representative lung tumor motion traces recorded from four patients using the Synchrony system [4]. The traces are indicative of the wide variety of respiratory patterns that are observed clinically.

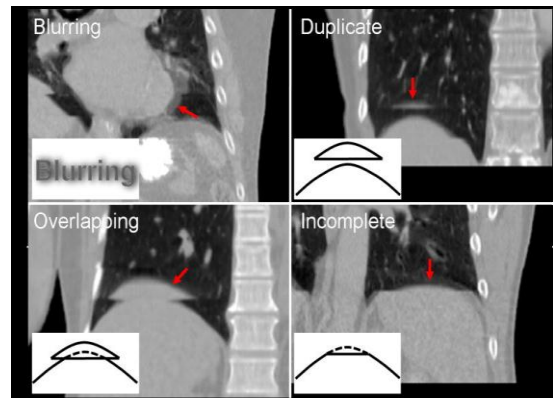


**Figure 3.** Examples of motion-induced artifacts observed in lung 4DCT [5].

While a variety of strategies have been proposed to improve 4DCT-based planning and delivery paradigm, several fundamentally challenging issues need to be tackled:

- i) As seen in Fig. 2, respiratory motion is much more complex than can be characterized by a single cycle. Such cycle-to-cycle complexities are unaccounted for in the MIP and AIP images and can lead to errors [6].
- ii) Forcing CT projection data acquired over several cycles into a few respiratory phase bins can lead to severe artifacts (Fig. 3). Yamamoto et. al. found that 45 of 50 patients had at least one artifact, with a mean magnitude of 11.6 mm (range: 4.4 - 56.0 mm) [5].
- iii) The equivalent dose for 4DCT is quite high (29 - 40 mSv), about 4 times higher than that for 3DCT (3 - 10 mSv) [7]. Such high imaging dose discourages more frequent imaging and long-term monitoring.

### 3. Need for Development

Therefore, it is highly desirable to have a computational RT-guidance strategy where a 4D motion model is developed from 4D MRI and a planning 3DCT acquired at a reference phase. During delivery, the model is updated with real-time position information. The correspondingly updated fluence map can then be delivered.

### 4. Computational Framework

In order to accurately model the tumor and surrounding sensitive structures, we build a geometric modeling framework that tackles several important 3D image analyses and processing tasks. Irradiation volume is parameterized temporally using a 4D model. A tight planning margin could be extracted from this deforming 4D parametric model, to spare normal tissues from dose radiation during delivery. We propose a framework has two phases (see the right chart):

- (1) Offline Planning: based on CT and MR scans, a deforming 4D parametric model  $M(x,y,z,t)$  is constructed to mimic the trajectory and deformation of the irradiated volume (IV).
- (2) Online delivery: real-time scanned 2D-

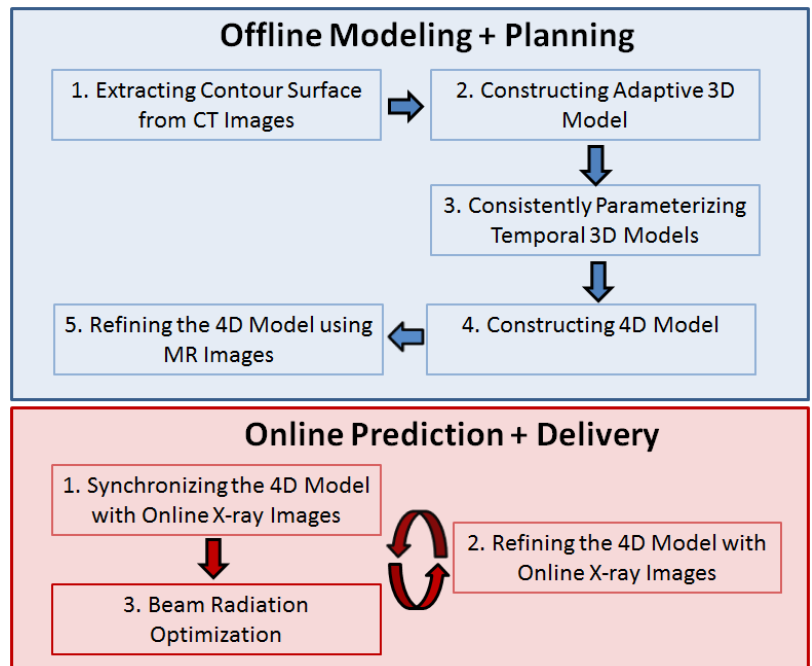


**Figure 4.** Computational Framework for Tumor Modeling and Radiation Treatment Planning.

images (orthogonally mounted kV x-ray) are used to synchronize and refine the 4D model. The 4D model is used to predict trajectory and geometry of the tumor, and facilitates the optimization for treatment beam, which shall move to the most desirable radiation positions.

#### 4.1 Planning Stage: Constructing the 4D Model

In the offline phase, we model the motion and deformation of the tumor. To better predict its movement, which could be affected by neighboring organs/tissues during their respiration movements, we shall model the entire neighboring volume region.

##### 1) Contour Segmentation (CT Image Stacks → Surface Contours)

We first segment the tumor and surrounding structures within the potential irradiated volume from 3D CT/MR images clearly. Reliable 3D image segmentation against noise is critical here. We propose an algorithm based on interactive graph cut pre-segmentation plus an active-contour post-refinement. The 3D graph-cut is performed on a novel metric combining (1) intensity of the image (with noise filtered) and (2) a pre-designed implicit scalar field capturing the template shape (serving as a reference). The graph-cut algorithm reaches the globally optimal segmentation; the extracted contour can be iteratively and adaptively refined via simple user

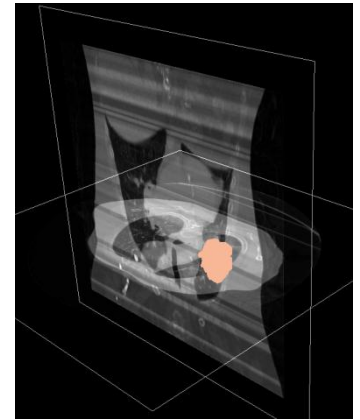
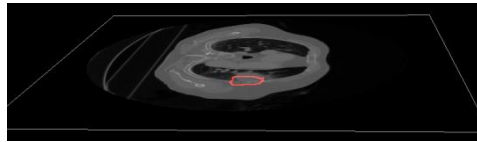


**Figure 5.** Tumor Segmentation from the CT Images. (Right) Segmentation performed in 3D; the red solid is the tumor; (Left) segmentation visualized in a cross section.

interactions. Then finally we perform variational fairing over these contours using some specific smoothness energy defined for biomembranes.

Preliminary experiments (Fig. 5, Fig. 6) demonstrate that our segmentation (a) is superior over other popular segmentation methods (b-e). A runtime table is also shown following the figure, which indicates our segmentation is efficient.

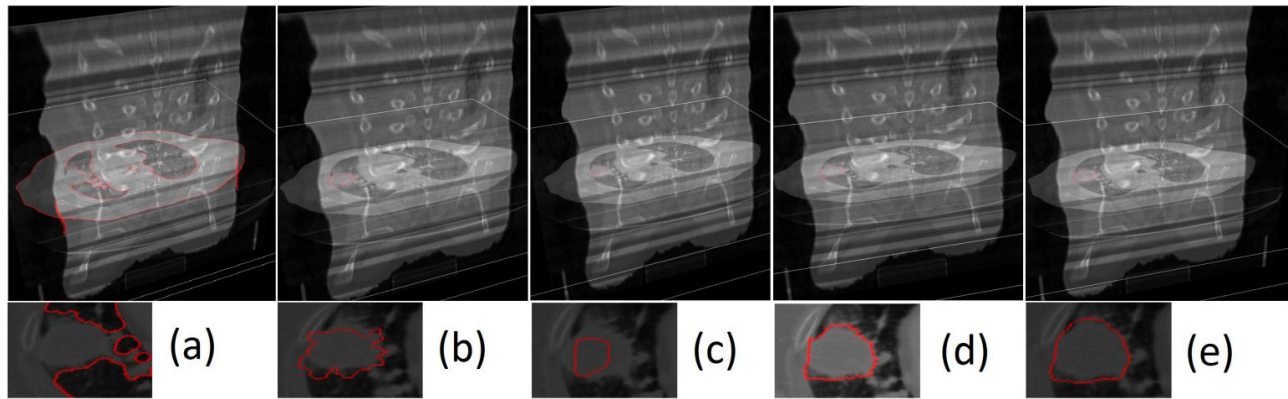


**Figure 6. Segmentation Results Comparison.** Tumor contour segmentation based on (a) level set methods [8,9] (a), watershed method [10] (b), original graph cut method [11] (c), and template-guided graph cut method without de-noise (d) and with de-noise (e). The final segmentation (e) is suitable for subsequent tumor modeling and tracking tasks.

Data / Time (seconds)	Level set	Watershed	Graph Cut
4DCT_Disc1_SE1	47.186759	1.844548	15.551345
4DCT_Disc1_SE8	58.906006	1.424914	16.741550

## 2) Adaptive Tetrahedralization (2D manifolds $\rightarrow$ 3D manifolds)

After extracting contours of both the tumor and surrounding structures, both geometry and material of the entire volume (instead of only boundary shells) should be modeled. We then adaptively tessellate the irradiated volume to obtain a tetrahedral mesh.

Such a finite element representation is much sparser than the grid-based image representation, and any local region can be coarsened or refined adaptively when necessary. This effectively represents the inherent structure of the region, while

conforming to important features/materials.

The deforming IV can then be represented by a linear spline over this tetrahedralization.

One critical issue is to compute the optimal sampling points for the tessellation.

We formulate this problem as minimizing the peak signal to noise ratio (PSNR) subject to a given budget number of points, where the mean square error (MSE) is the absolute difference between original and interpolated grey values. Intuitively, selected points balance the uniformity and the sampling of sharp features. Once the sampling points are computed, the tessellation can be constructed using constrained Delaunay tetrahedralization, and then a unique spline space can be constructed upon this mesh. Fig. 7 illustrates an example of the tetrahedral representation of tumor and the surrounding tissue.

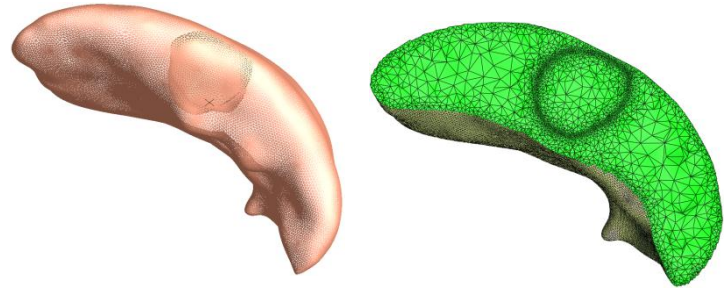


**Figure 7.** Tumor and Right Lung. (Left) Contour Surfaces; (Right) Adaptive Tetrahedralization.

## 3) Volumetric Registration and Interpolation (3D volumes $\rightarrow$ 4D IV)

After volumetric regions of interest are represented using tetrahedral meshes, we compute bijective volumetric mapping to consistently parameterize 3D volumes; then we interpolate the 4D temporal model.

First, we compute the low-distorted mapping between two consecutive volumes through a coarse to fine framework. First, corresponding features can be extracted and matched in 3D; and since a robust correspondence against geometric disparity is desirable, we can use features such as 3D heat kernel functions to design variant scale spaces. Globally optimal surface [13,14] and volumetric mapping [15,16], taking these features as soft constraints, can be computed between corresponding contours and volumes. All temporally sequential volumes are now consistently parameterized onto one common domain  $D(u,v,w)$ .

Second, with one-to-one correspondence, we compute physically natural shape interpolation between two consequent models, to form a continuously deforming 4D model:  $M(u,v,w,t)$ . It can be continuously interpolated: given  $(u,v,w)$  parameter coordinate in the domain, we can trace a point's trajectory under different time  $t$ ; similarly, given any  $t$ , we obtain the 3D volume's location and geometry at that moment.

## 4) Refining the 4D Model using MRI (4D IV $\rightarrow$ Parametric Periodic Model)

The above steps 1 to 3 are performed based on CT images, whose resolution can be very high and the accuracy can be very nice. But due to its high dose, frequent and long-sequence of CT imaging is impossible. CT sampled volumes are therefore sparse and few. We refine this 4D model using a sequence of 3D MR images. Cross-model volumetric parameterization can again be used to register the volume from the MRI and the interpolated volume. We correct the consistently deforming 4D model according to this matching result. The refined continuous parametric 4D model is ready to be used for determining the trajectory and geometry of the interested volume.

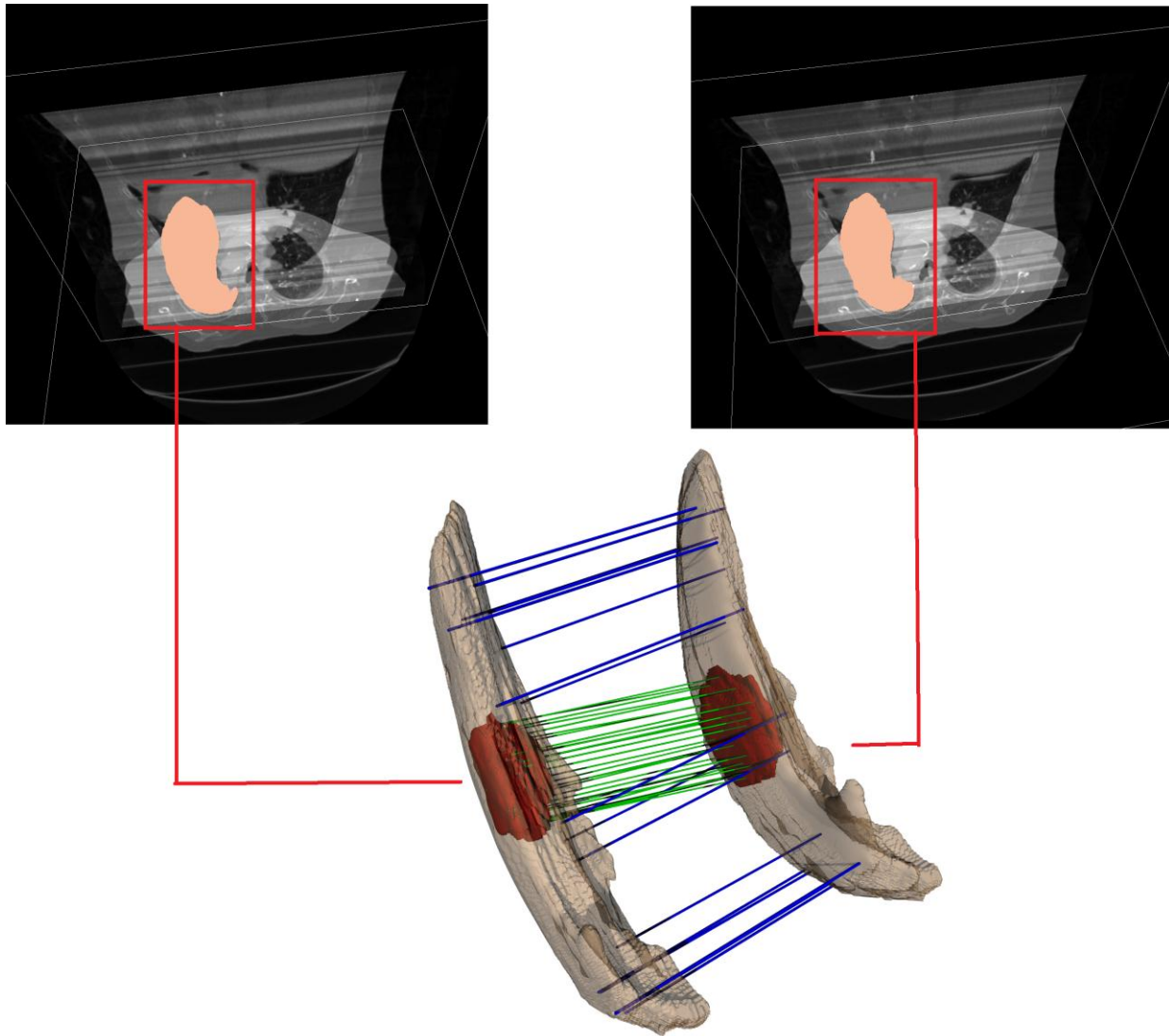


**Figure 8.** Tracking Temporally Deforming Tumor and Surrounding Lobe. The red solids represent the tumor under two time sequences, while green and blue lines indicate the correspondence between temporally deforming geometry of this local region.

#### 4.2 Delivery Stage: 4D Model Refinement and Motion Prediction

##### 1) Synchronizing/Refining the 4D Model using X-ray Images

During the delivery stage, a 2D X-ray projection image can be obtained. We register it with the moving 3D model and use the matching to correct the 4D model. The optimal mapping can be searched within a conservative time range, starting from the last synchronized point.

##### 2) Beam Radiation Optimization

With the deforming 3D volume, we can optimize the optimal radiation direction of the beam. Ideally the beam should be planed so that it can see the tumor clearly, without being visually blocked by other organs, because otherwise the radiation will hit those organs before it reaches the tumor. Therefore, finding best spots of the beam can be solved, we propose to use an efficient hierarchical integer linear programming (HILP) to solve this problem. Such a proposed novel HILP scheme has been demonstrated very efficient in solving the challenging 3D region guarding problem in our recent work in autonomous robotic environment inspection [17].

Performance of the algorithms in the above entire pipeline can be further improved using parallel scheme on GPU, which can be effectively improved by 20 to 100 times.

## 5. Conclusion

We propose a novel potential computational framework for lung tumor modeling and tracking. The paradigm can be used for radiotherapy (RT) planning and delivery optimization. The proposed framework effectively integrates an entire pipeline including reliable 3D image segmentation, volumetric modeling, analysis, and parameterization, accurate physical/geometric interpolation and tracking techniques. The computation performance of this framework can be further improved using parallel scheme on GPU, to achieve a significant efficiency improvement (20 to 100 times) for both offline data analysis and planning and real-time treatment optimization.

## References

- 1 G. S. Mageras, A. Pevsner, E. D. Yorke, K. E. Rosenzweig, E. C. Ford, A. Hertanto, S. M. Larson, D. M. Lovelock, Y. E. Erdi, S. A. Nehmeh, J. L. Humm, and C. C. Ling, "Measurement of lung tumor motion using respiration-correlated CT," *Int J Radiat Oncol Biol Phys* **60** (3):933-941, 2004.
- 2 N. Wink, C. Panknin, and T. D. Solberg, "Phase versus amplitude sorting of 4D-CT data," *J Appl Clin Med Phys* **7**(1):77-85, 2006.
- 3 E. Rietzel, A. K. Liu, G. T. Chen, and N. C. Choi, "Maximum-intensity volumes for fast contouring of lung tumors including respiratory motion in 4DCT planning," *Int J Radiat Oncol Biol Phys* **71**(4):1245-1252, 2008.
- 4 Y. Suh, S. Dieterich, B. Cho, and P. J. Keall, "An Analysis of Thoracic and Abdominal Tumour Motion for Stereotactic Body Radiotherapy Patients," *Phys Med Biol* **53**:3623-3640, 2008.
- 5 T. Yamamoto, U. Langner, B. W. Loo, Jr., J. Shen, and P. J. Keall, "Retrospective analysis of artifacts in four-dimensional CT images of 50 abdominal and thoracic radiotherapy patients," *Int J Radiat Oncol Biol Phys* **72** (4):1250-1258, 2008.
- 6 J. Cai, P. W. Read, J. M. Baisden, J. M. Larner, S. H. Benedict, and K. Sheng, "Estimation of error in maximal intensity projection-based internal target volume of lung tumors: a simulation and comparison study using dynamic magnetic resonance imaging," *Int J Radiat Oncol Biol Phys* **69**(3):895-902, 2007.
- 7 S. Mori, S. Ko, T. Ishii, and K. Nishizawa, "Effective doses in four-dimensional computed tomography for lung radiotherapy planning," *Med Dosim* **34**(1):87-90, 2009.
- 8 Chan, T.F; Vese, L.A; Active contours without edges. *IEEE Transactions on Image Processing*, Vol.10. pp. 266-277, 2001.
- 9 Xiao-Feng Wang, De-Shuang Huang, Huanhuan Xu, "An Efficient Local Chan-Vese Model for Image Segmentation," *Pattern Recognition*. 43(3), pp.603-618, 2010.
- 10 Meyer, Fernand, "Topographic distance and watershed lines," *Signal Processing*, Vol. 38, July 1994, pp. 113-125
- 11 Yuri Boykov, Gareth Funka-Lea, Graph Cuts and Efficient N-D Image Segmentation. *International Journal of Computer Vision*, Vol.70, Nov. 2006. Pp. 109—131.
- 12 Jian Sun, Maks Ovsjanikov and Leonidas Guibas, "A Concise and Provably Informative Multi-Scale Signature Based on Heat Diffusion", *Comput. Graph. Forum*, Volume 28 Issue 5, pages 1383-1392, 2009.
- 13 X. Li, Y. Bao, X. Guo, M. Jin, X. Gu, and H. Qin, "Globally Optimal Surface Mapping for Shapes of Arbitrary Topology", *IEEE Trans. on Visualization and Computer Graphics*, Vol. 14, No. 4, pp. 805-819, 2008.

14. X. Li, X. Gu, H. Qin, "Surface Mapping using Consistent Pants Decomposition", IEEE Trans. on Visualization and Computer Graphics (TVCG), Vol. 15, No. 4, pp. 558-571, 2009.
15. Xin Li, Xiaohu Guo, Hongyu Wang, Ying He, Xianfeng Gu, and Hong Qin, "Meshless Harmonic Volumetric Mapping using Fundamental Solution Methods", IEEE Trans. on Automation Science and Engineering, Vol. 6, Issue 3, pp. 409 - 422, 2009.
16. Xin Li, Huan huan Xu, Shenghua Wan, Zhao Yin and Wuyi Yu , Feature-aligned Harmonic Volumetric Mapping using MFS ,Comp. & Graph., Vol. 34, No. 3, pp. 242-251, 2010.
17. X. Li, W. Yu, X. Lin, and S. Iyengar, "Optimizing Autonomous Pipeline Inspection", IEEE Trans. on Robotics, to appear, 2011.